analytical chemistry

pubs.acs.org/ac Article

Ultrasensitive and Visual Electrochemiluminescence Ratiometry Based on a Constant Resistor-Integrated Bipolar Electrode for MicroRNA Detection

Jie Zhao, Chuan-Xiang Chen,* Jia-Wan Zhu, Hui-Long Zong, Yong-Hong Hu,* and Yin-Zhu Wang*

Cite This: *Anal. Chem.* 2022, 94, 4303−4310 Read Online

ACCESS | Metrics & More | Article Recommendations | Supporting Information

ABSTRACT: In this work, a new electrochemiluminescence (ECL) platform was constructed for detecting the prostate cancer marker microRNA-141 (miRNA-141) on a constant resistor-integrated closed bipolar electrode (BPE). It consisted of two reservoirs and a constant resistor, and both ends were connected to the anode of the driving electrode and the cathode of BPE. The cathode of BPE was modified with boron nitride quantum dots (BNQDs), and the anode reservoir was the $[Ru(bpy)_3](PF_6)_2$/TPrA system. After introducing a certain amount of hairpin DNA 3 (H3) and ferrocene-labeled single-stranded DNA (Fc-ssDNA) on the surface of the BNQDs, the ECL emission signal of the BNQDs was difficult to be observed by the naked eye, while $[Ru(bpy)_3](PF_6)_2$ emitted a strong and visible ECL signal. In the presence of the target, bipedal DNA assembled by catalytic hairpin assembly (CHA) took away the Fc-ssDNA and the ECL intensity of the BNQDs was enlarged, and as the concentration of miRNA-141 increased to the cutoff value, yellow-green light was visible by the naked eye. Meanwhile, the red emission signal of $[Ru(bpy)_3](PF_6)_2$/TPrA became weakened. Thus, an ultrasensitive "color switch" ECL biosensor for detection of miRNA-141 was constructed and endowed with a wide linear range from 10^{-17} to 10^{-7} M and a detection limit of 10^{-17} M (S/N = 3). This study provides the potential for investigating portable devices in the detection of low-concentration nucleic acids.

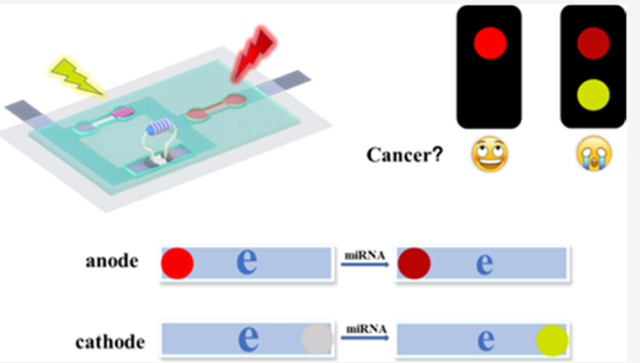

INTRODUCTION

MicroRNA (miRNA) is a small single-stranded molecule composed of 19−24 nucleotides, which plays a vital role in various life activities of organisms.[1−3] It can serve as an essential regulator in tissue differentiation, proliferation, and hematopoiesis.[4] Previous works have indicated that the abnormal expression of miRNA is related to the occurrence of various cancers, such as the abnormal expression (down- or upregulation) of microRNA-141 (miRNA-141) correlating with various types of human cancers, including cancers of prostate, breast, ovarian, colorectal, pancreatic, and others.[5] Therefore, the detection of miRNA in the human body is meaningful for the diagnosis and prognosis of cancer. Traditional analysis methods, including fluorescence,[4] northern blot hybridization,[6] and real-time quantitative polymerase chain reaction (qRT-PCR),[7] are widely used to detect miRNA. However, there are some shortcomings: (i) although the fluorescence system can obtain intuitive results by imaging, the instrument is large and expensive; (ii) nonspecific amplification during qRT-PCR is also prone to false positives; and (iii) the northern blot hybridization method requires a large number of samples and could not be used for the determination of low-abundance miRNAs.[8] Therefore, it is important to develop an intuitive, accurate, and ultrasensitive miRNA detection strategy.

Electrochemiluminescence (ECL) is a phenomenon in which molecules or quantum dots are oxidized or reduced on the electrode surface to form a photon emission state, which leads to luminescence upon returning to the ground state.[9−12] Compared to the traditional single-signal ECL measurement, the ratiometric ECL regulates environmental changes by self-calibrating the ratio of two signals and effectively avoids the interference of external factors on the traditional molecular probe signal.[13] For ECL systems, since the optical signal is measured, if the optical signal is strong enough, it can be visualized and read out directly by the naked eye without additional signal readout devices, making analysis and detection simpler.[14] Combining the advantages of ratiometric and visual ECL, Zhang et al.[15] designed a type of

Received: November 15, 2021
Accepted: February 18, 2022
Published: March 1, 2022

Downloaded via UNIV OF GLASGOW on November 7, 2022 at 19:16:05 (UTC).
See https://pubs.acs.org/sharingguidelines for options on how to legitimately share published articles.

ACS Publications © 2022 American Chemical Society

https://doi.org/10.1021/acs.analchem.1c04971
Anal. Chem. 2022, 94, 4303−4310

Scheme 1. Schematic Diagram of the Ultrasensitive "Color Switch" ECL Ratiometric Biosensor Based on the Constant Resistor-Integrated BPE

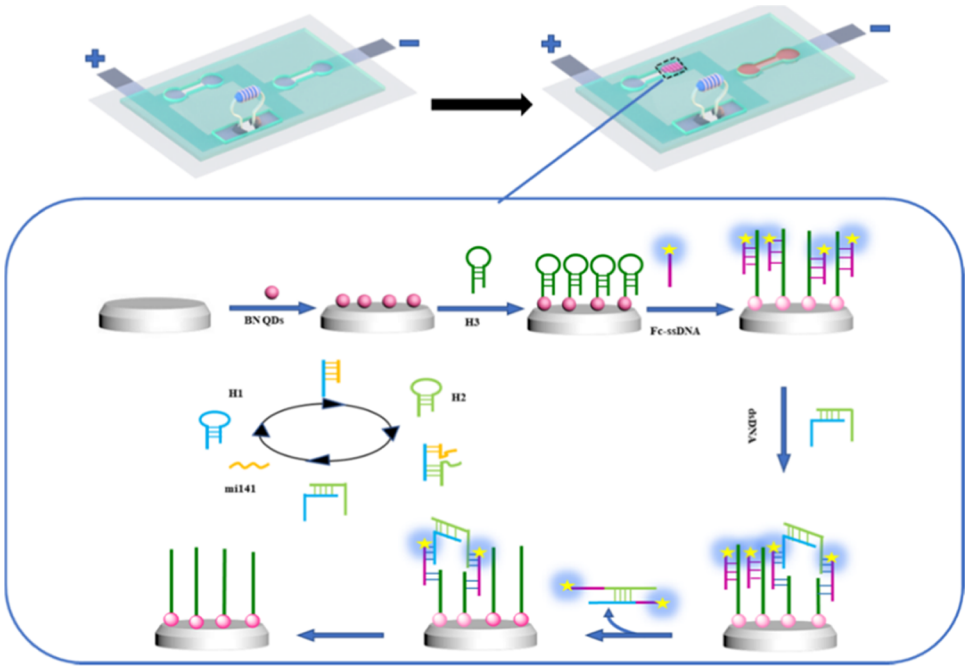

dual bipolar electrode (BPE) chip that could give ECL signals of different colors for the detection of HL-60 cancer cells, which not only improved the accuracy of ECL detection but also used for intuitive tumor recognition. BPE is a conductive material immersed in an electrolyte with an electrochemical reaction at its two ends at a sufficient driving voltage. As a kind of BPE, a "closed" BPE system physically separates the solutions contacting the two poles of the BPE, with only a current path between the two half-cells.[16,17] Such a "closed" BPE structure was often used to fabricate ratiometric and visual ECL biosensors since different ECL reactions could be performed in separated cells.[15] However, at present, these types of biosensors cannot achieve ultrasensitive detection of miRNA, mainly due to the limited selection of ECL reagents with high quantum yield, visible ECL intensity, and insufficient current flowing through BPE. Therefore, synthesizing ECL reagents with high quantum yield and visible light intensity and assisting highly efficient amplification technology to greatly improve the sensitivity of ratiometric and visual BPE-ECL biosensors have become the primary problem to solve the ultrasensitive detection of miRNA.

Boron nitride quantum dots (BNQDs) are zero-dimensional nanomaterials with high quantum yield and chemical stability,[18−20] which might be one of the most promising ECL emitters.[19] Except for selecting BNQDs as the cathode ECL reagent, we also need to choose a suitable anode ECL reagent to satisfy the complete separation of potential and wavelength from the BNQDs. At present, the ECL materials commonly used for anode visualization include luminol,[21] gold nanoclusters,[22] polymer dots,[23] ruthenium pyridine complex,[24] etc. $[Ru(bpy)_3](PF_6)_2$, belonging to ruthenium pyridine complexes, has a high quantum yield and its potential and wavelength could be completely separated from BNQDs. The red light emitted by this material is in strong contrast with the yellow-green light emitted by BNQDs, making the detection results colorful and easy to observe. Therefore, $[Ru(bpy)_3](PF_6)_2$ can be chosen as the anode luminescent material.[25,26]

An efficient signal amplification strategy was also a prerequisite for ultrasensitive detection of miRNAs. Traditional signal amplification techniques, including hybridization chain reaction,[27,28] rolling circle amplification,[29] strand displacement amplification,[30,31] and other amplification reactions,[32] usually face complex and subtle processes, which may bring great uncertainty to the accuracy of the results. Inspired by the fact that the parallel resistance can reduce the total resistance in the circuit and increase the total current (i_{tot}) in the circuit, we introduced a constant resistance in parallel with the BPE cathode in BPE to make the resistance of the whole circuit smaller, giving an advantage in driving voltage compared to the previous work,[33] thereby enhancing the ECL signal and improving the detection sensitivity under a specific driving voltage.

Taken together, to develop an intuitive, accurate, and ultrasensitive miRNA detection technique, we constructed an ultrasensitive "color switch" ECL biosensor based on the constant resistor-integrated BPE (Scheme 1). First, BNQDs were modified on the surface of the BPE cathode. A constant resistor was connected to the cathode of BPE, and the driving electrode with $[Ru(bpy)_3](PF_6)_2$/TPrA was added to the anode reservoir. After a large amount of hairpin DNA 3 (H3) and ferrocene-labeled single-stranded DNA (Fc-ssDNA) were incubated onto the surface of BNQDs, the emission of BNQDs was difficult to observe by the naked eye since Fc quenched the signal of BNQDs. However, $[Ru(bpy)_3](PF_6)_2$ emitted a strong red ECL signal on account of the increase of electron transfer in the circuit. At this time, there was only one visual signal in the circuit. At last, bipedal DNA assembled by catalytic hairpin assembly (CHA) was introduced onto the cathode of BPE and complemented ssDNA to take it away so that the quencher Fc would be far away from the electrode surface, resulting in the partial recovery of the ECL signal of

https://doi.org/10.1021/acs.analchem.1c04971
Anal. Chem. 2022, 94, 4303−4310

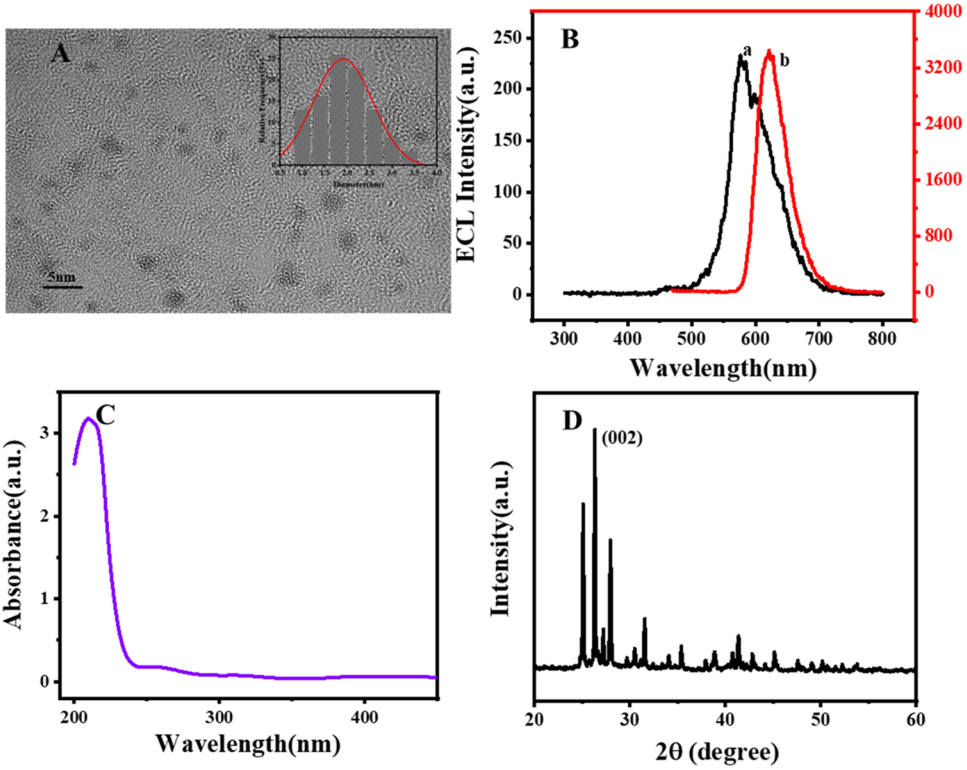

Figure 1. (A) TEM image of BNQDs; (B) ECL spectra of BNQDs (a) and $[Ru(bpy)_3](PF_6)_2$ (b); (C) UV−vis spectrum of BNQDs; and (D) XRD patterns of BNQDs.

BNQDs. We optimized the experimental conditions to make the ECL intensity of BNQDs visible by the naked eye when the target concentration of miRNA-141 was at the cutoff value. As the Fc on the electrode surface falls off, the total current (i_{tot}) decreases, resulting in the attenuation of the red emission. However, since $[Ru(bpy)_3](PF_6)_2$ had a strong ECL signal, even if the intensity became weak, the signal was still visible. There were two visual signals in the circuit at this point. Therefore, we could directly judge prostate cancer by the naked eye according to the number of signals in the circuit. Finally, the intensity ratio of $[Ru(bpy)_3](PF_6)_2$ and BNQDs was calculated to quantify the concentration of miRNA-141 of different regions, which significantly improved the sensitivity and the accuracy of early diagnosis of prostate cancer.

EXPERIMENTAL SECTION

Preparation of BNQDs. In this study, BNQDs were synthesized by a modified hydrothermal method.[34] First, 1.2 g of HBO_3 was added into 30 mL of ultrapure water and ultrasonicated for about 5 min to obtain a homogeneous solution. Then, 2.4 mL of concentrated ammonia was added with stirring, and the obtained solution was transferred to a Teflon-lined autoclave and heated to 200 °C for 12 h. After the reaction, the reaction kettle was cooled to obtain a uniform and transparent solution, and its pH value was adjusted to 7.0 by 0.1 M HCl. After centrifugation, the resulting product was stored at 4 °C.

Manufacture of the ITO Working Electrode and BPE. A piece of ITO glass was ultrasonically cleaned with acetone, ethanol, and water boiled in isopropyl alcohol containing 2 M KOH hydroxide for 15 min and then dried at 120 °C. A piece of transparent tape (6 mm diameter) was punched and stuck on the ITO surface to form a working surface, providing an effective area for electrochemical measurements. The specific preparation process of BPE was as follows: For screen printing, first, ITO glass was cut into small pieces (6.5 cm × 1 cm), and then the designed template was printed on the ITO surface with ink under the printing effect to form the desired electrode shape. Next, the ITO glasses were immersed in a 2 M KOH/100 mL isopropyl alcohol solution and boiled for 20 min, followed by washing with water. To obtain the PDMS molds, an SG-2506 borosilicate glass plate was covered with a designed mask and exposed to ultraviolet (UV) light for 2 min and then soaked and cleaned with a 0.5% NaOH solution. The Cr layer was then removed by a 0.2 M solution of ammonium cerium nitrate. Etching of these glass plates was carried out in a solution of 1 M HF-NH_4F at 40 °C for 35 min. After etching, designed channel structure molds were obtained. Then, degassed PDMS was cast on these glass masks for 1 h at 80 °C (the ratio of the PDMS monomer to the curing agent was 1:10). After cooling at room temperature, PDMS was stripped from the masks, producing the PDMS molds. The PDMS molds were attached to the ITO-coated glass slice (circular holes as reservoirs and the square hole for connecting to the resistor).

CHA-Driven Target Amplification Process. First, hairpin DNA 1 (H1, 2 μM) and hairpin DNA 2 (H2, 2 μM) were slowly annealed at 95 °C for 5 min and cooled to 25 °C to form a hairpin structure. Then, the equal volumes of H1 and H2 were reacted with different concentrations of miRNA-141 and maintained for 40 min at room temperature to obtain dsDNA (H1−H2). In this progress, H1 was first opened when adding target miRNA-141. After that, the exposed partial complementary sequence was used to further hybridize with H2 to displace miRNA-141 and form into dsDNA. Finally, the

https://doi.org/10.1021/acs.analchem.1c04971
Anal. Chem. 2022, 94, 4303−4310

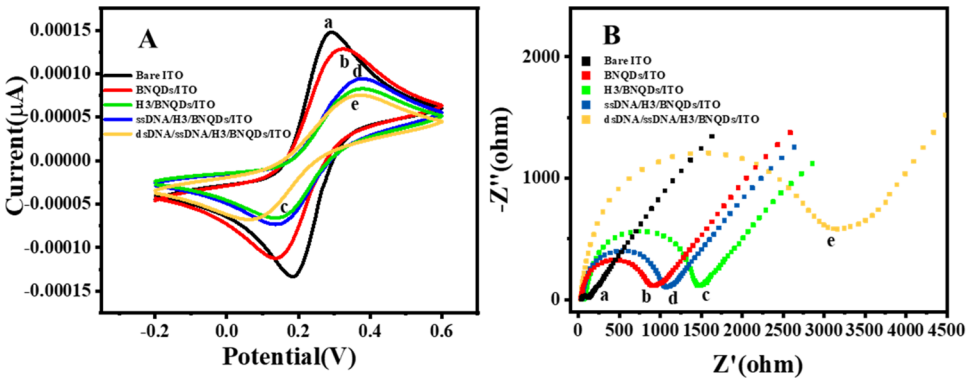

Figure 2. CV (A) and EIS (B) diagrams of the electrode in the process ((a) bare ITO, (b) BNQDs/ITO, (c) H3/BNQDs/ITO, (d) ssDNA/H3/BNQDs/ITO, (e) dsDNA/ssDNA/H3/BNQDs/ITO). CVs of the proposed biosensor were carried out from −0.2 to 0.6 V in a 5 mM $[Fe(CN)_6]^{3-/4-}$ solution containing 0.1 M KCl. The scan rate is 100 $mV{\cdot}s^{-1}$.

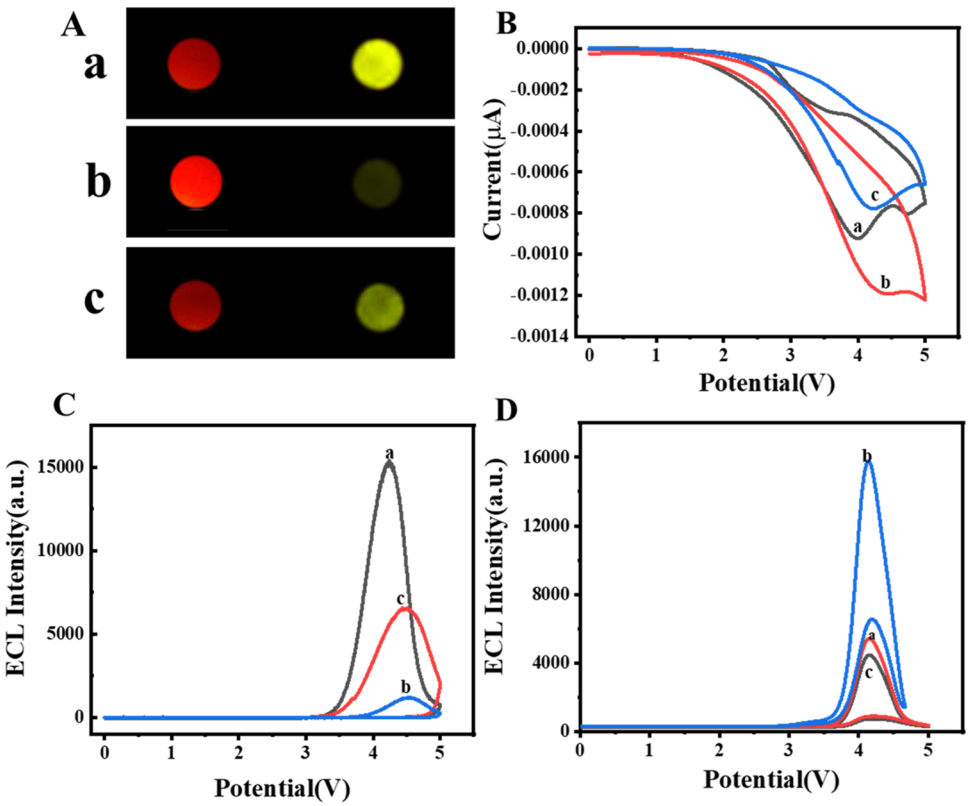

Figure 3. ECL images (A) and corresponding CV curves (B) of BPE. ECL response of the cathode (C) and anode (D) of the constructed process of the ultrasensitive "color switch" ECL biosensor. ((a) BNQDs/ITO, (b) Fc/BNQDs/ITO, (c) dsDNA/Fc/BNQDs/ITO). The scan rate is 100 $mV{\cdot}s^{-1}$ with a voltage of PMT = 400 V, with the potential scan from 0 to 5.0 V.

released miRNA-141 could be recycled to trigger the next CHA for achieving signal amplification.

Target Detection. First, 20 μL of BNQD solution (0.04 g/mL) was dropped on the cathode of BPE and dried naturally to form a thin film. Then, 10 μL of 2 μM hairpin DNA 3 (H3) was dropped on the film and incubated for 12 h at 4 °C. Next, 5 μL of a 1.0 mM BSA solution was incubated for 40 min to block nonspecific adsorption sites. Then, ferrocene-labeled single-stranded DNA (Fc-ssDNA, 10 μL, 2.0 μM) was incubated on the cathode of BPE for 2 h at 37 °C. Subsequently, the prepared dsDNA (20 μL) was dropped on the cathode of BPE and maintained for 60 min. Finally, 0.1 M PBS (pH = 7.4) containing 0.1 M $K_2S_2O_8$ was added into the cathodic reservoir. ECL images were taken with an Olympus DP71 CCD camera; meanwhile, i_{tot} was recorded. The ECL spectrum was recorded based on a three-electrode system on a CHI 660C electrochemical workstation combined with an F7000 fluorescence spectrometer (Hitachi, Japan). All experiments were carried out at room temperature.

RESULTS AND DISCUSSION

Characterization of BNQDs and $[Ru(bpy)_3](PF_6)_2$. The morphology of the BNQDs was characterized using a transmission electron microscope (TEM). As shown in Figure 1A, it could be clearly observed that the prepared BNQDs displayed relatively uniform spherical particle size with a diameter of about 1.95 ± 0.62 nm, which was consistent with the previous report.[35] Figure 1B shows the ECL emission

https://doi.org/10.1021/acs.analchem.1c04971
Anal. Chem. 2022, 94, 4303−4310

spectra of BNQDs and $[Ru(bpy)_3](PF_6)_2$. The dispersion of curve a showed a strong ECL emission peak centered at about 575 nm, and $[Ru(bpy)_3](PF_6)_2$ had an ECL peak of about 620 nm (curve b), which were consistent with the previous reports.[36,37] The ultraviolet−visible absorption spectrum (UV−vis) of BNQDs in Figure 1C had a significant peak at 215 nm from the $\pi-\pi^*$ conjugated structures existing in the QDs. There are many boron and carbon atoms in BNQDs, and the alternate positioning of the two atoms can form a two-dimensional conjugate layer. The B−N rings were similar to the configuration of the benzene molecule, thereby rendering many $\pi-\pi^*$ conjugated structures.[34,38,39] The X-ray diffraction (XRD) pattern of BNQDs showed that the main peak located at $2\theta = 26.3°$ corresponded to the (002) plane (Figure 1D).[18]

CV and EIS Characterization of the Biosensor Structure. Cyclic voltammetry (CV) and electrochemical impedance spectroscopy (EIS) were applied to verify the successful construction of the biosensor. The fabrication process of the biosensor was characterized by CV and EIS in a 5.0 mM $[Fe(CN)_6]^{3-/4-}$ solution consisting of 0.1 M KCl where ITO was used as the working electrode, platinum wire as the auxiliary electrode, and Ag/AgCl (saturated KCl) as the reference electrode. According to the CV curves shown in Figure 2A, the bare ITO (curve a) displayed a pair of reversible redox peaks, indicating a fast electron transfer process of the $Fe(CN)_6^{3-/4-}$ redox system. Compared with bare ITO, the redox currents of the BNQD modified electrode declined to some extent (curve b) owing to the hindrance of BNQDs for electron transport. After H3 was incubated on the electrode, curve c revealed that redox currents decreased since DNA could hinder the transmission of electrons. Then, the redox currents also increased (curve d) when Fc-ssDNA was incubated on the electrode surface because of the electro-oxidation of Fc to Fc^+, which would accelerate electron transfer. But after incubating with dsDNA, the redox currents decreased (curve e), which was attributed to the fact that the negatively charged DNA hindered electron transfer.

EIS was used to characterize the assembly process of biosensors. The electron transfer resistances (R_{et}) of $[Fe(CN)_6]^{3-/4-}$ of different modified electrodes are shown in Figure 2B. Curve a showed that bare ITO afforded a small semicircle, indicating a low R_{et} value. After BNQDs were attached to the electrode, the semicircle significantly increased due to the hindrance of BNQDs for electron transport (curve b). When H3 was modified on the electrode, R_{et} increased (curve c). However, R_{et} decreased with the immobilization of Fc-ssDNA on the electrode surface (curve d) owing to the fast electron transfer determined by Fc. Then, R_{et} increased obviously when dsDNA was incubated on the electrode surface (curve e). The above results were consistent with the current changes in Figure 2A, indicating the successful preparation of the biosensor.

Detection Principle of the Visual Biosensor. The operation procedures of BPE-ECL are schematically depicted in Scheme 1, and the corresponding ECL images, current versus potential, and intensity versus potential are shown in Figure 3. In the beginning, the cathode of the BPE was modified with 0.04 g/mL BNQDs, and 3.0 mM $[Ru(bpy)_3](PF_6)_2$/25 mM TPrA was added to the anode reservoir. The driving voltage was 5.0 V, and dual-color light bands were observed on both the cathode and anode of BPE (Figure 3A,a). The red band was ascribed to an ECL reaction of $[Ru(bpy)_3](PF_6)_2$/TPrA. In the $[Ru(bpy)_3](PF_6)_2$/TPrA system, the signal was generated by the reaction between $[Ru(bpy)_3](PF_6)_2$ and TPrA, and the related mechanism was depicted as follows

$$TPrA - e^- \rightarrow TPrA^{+\cdot} \quad (1)$$

$$TPrA^{+\cdot} \rightarrow TPrA^{\cdot} + H^+ \quad (2)$$

$$[Ru(bpy)_3]^{2+}(PF_6)_2 - e^- \rightarrow [Ru(bpy)_3]^{3+}(PF_6)_2 \quad (3)$$

$$[Ru(bpy)_3]^{3+}(PF_6)_2 + TPrA^{\cdot} \rightarrow [Ru(bpy)_3]^{2+}(PF_6)_2{}^* + P \quad (4)$$

$$[Ru(bpy)_3]^{2+}(PF_6)_2{}^* \rightarrow h\nu + [Ru(bpy)_3]^{2+}(PF_6)_2 \quad (5)$$

Moreover, the yellow-green light emission at the cathode of BPE was attributed to the ECL reaction of BNQDs-$K_2S_2O_8$. For the BNQDs/$S_2O_8^{2-}$ system, BNQDs were reduced to $BN^{-\cdot}$, the reduction of $S_2O_8^{2-}$ produces the strong oxidant $SO_4^{-\cdot}$, and $BN^{-\cdot}$could react with $SO_4^{-\cdot}$ to generate the signal.[38,40] The proposed ECL process is displayed in the Supporting Information.

After incubating H3 and Fc-ssDNA on the surface of BNQDs, the intensity of the yellow-green light band was reduced to be invisible by the naked eye since Fc quenched the emission of BNQDs (Figure 3A,b, right). The transfer of energy and electron between Fc and BNQDs* was supposed to be the main reason for the formed quenching effect.[41] Energy transfer occurred between Fc and BNQDs* (eq 6). Alternatively, Fc was oxidized to form ferrocene (Fc^+) by the strong oxidant $SO_4^{-\cdot}$ (eq 7). The oxidized species of Fc^+ could further react with e^- (eq 8) and then react with BNQDs* to directly quench the ECL emission of BNQDs through an electron transfer mechanism (eq 9). Therefore, we found that the yellow-green emission of BNQDs was too weak to be observed by the naked eye. The possible mechanisms were proposed in the following two pathways

$$Fc + BNQDs^* \rightarrow BNQDs + Fc^+ \quad (6)$$

or

$$Fc + SO_4^{-\cdot} \rightarrow SO_4^{2-} + Fc^+ \quad (7)$$

$$Fc^+ + e^- \rightarrow Fc \quad (8)$$

$$Fc + BNQDs^* \rightarrow BNQDs + Fc^+ \quad (9)$$

At the same time, the red band of $[Ru(bpy)_3](PF_6)_2$ became brighter (Figure 3A,b, left). Because we applied an external voltage of 5.0 V, Fc and BNQDs* reacted to generate Fc^+ at first. Then, $[Ru(bpy)_3](PF_6)_2$ and TPrA were oxidized at the ITO anode and emitted ECL. Moreover, Fc^+ and/or oxygen could be reduced at the cathode at the same rate. Since Fc^+ had a lower redox potential (0.74 V vs NHE) than oxygen (1.229 V vs NHE). Under a certain external voltage, the presence of Fc^+ on the cathode could promote the oxidation reaction on the anodic pole of the BPE, resulting in a significant increase of ECL intensity on the anode.[42] When dsDNA initiated by 10^{-14} M miRNA-141 was incubated on the cathode of the BPE, the intensity of the green-yellow light band of BNQDs/$K_2S_2O_8$ increased intensively (Figure 3A,c, right), which was attributed to the disassembly of Fc caused by the binding of dsDNA and ssDNA. Meanwhile, the anode emission of $[Ru(bpy)_3](PF_6)_2$/TPrA decreased (Figure 3A,c, left).

https://doi.org/10.1021/acs.analchem.1c04971
Anal. Chem. 2022, 94, 4303−4310

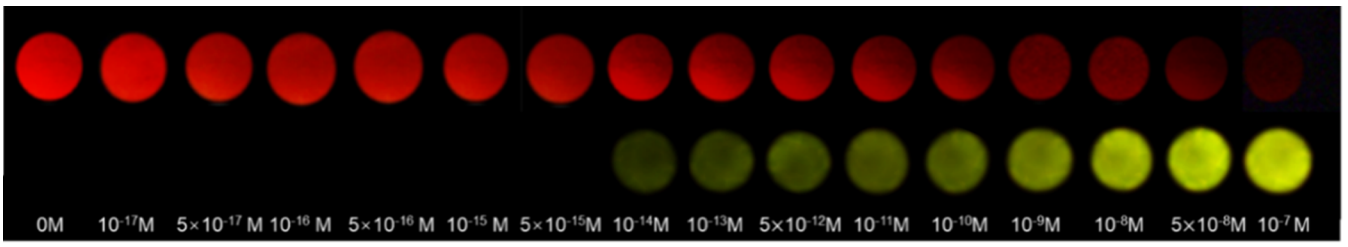

Figure 4. Visual ECL images of the designed biosensor in the presence of different concentrations of miRNA-141.

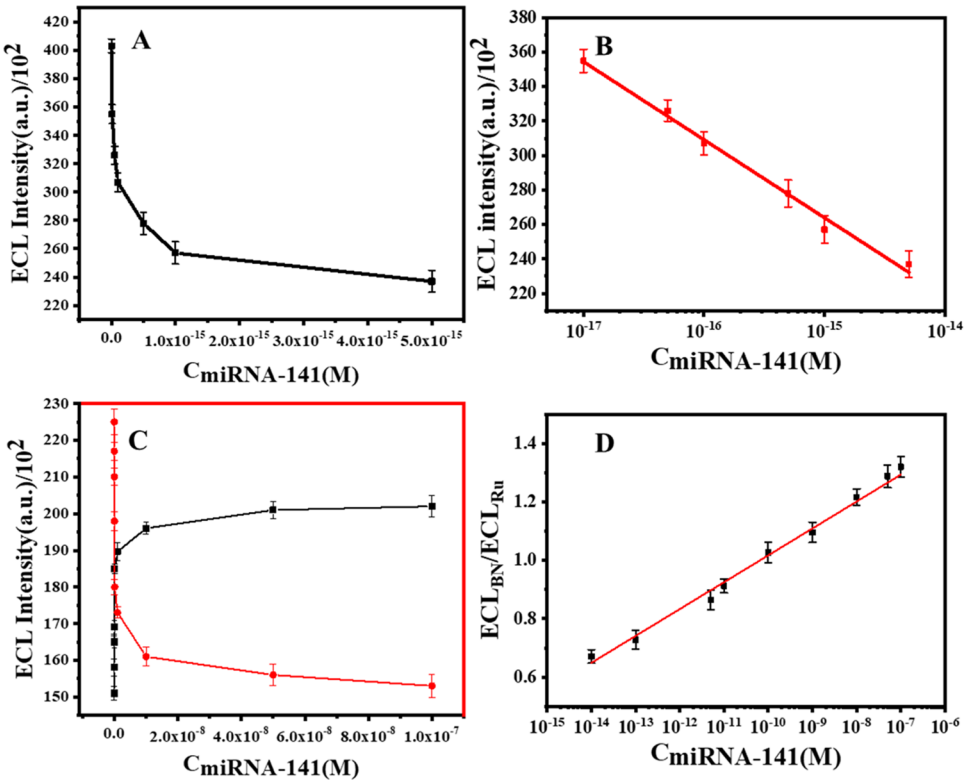

Figure 5. Corresponding intensity calibration curves (A, B) for detection of 0, 10^{-17}, 5×10^{-17}, 10^{-16}, 5×10^{-16}, 10^{-15}, and 5×10^{-15} M miRNA-141. The corresponding intensity calibration curves (C) and the linear relationship (D) between (ECL_{BN}/ECL_{Ru}) of the designed biosensor in the presence of different concentrations of 10^{-14}, 10^{-13}, 5×10^{-12}, 10^{-11}, 10^{-10}, 10^{-9}, 10^{-8}, 5×10^{-8}, and 10^{-7} M miRNA-141. Error bars represent the standard deviation from three independent experiments.

To gain more understanding of the sensing principle of our sensor, we considered the two poles of the BPE individually and compared the experimental results with the BPE system without the constant resistor. As shown in Figure 3C, during the potential scanning from 0 to 5.0 V, the ECL intensity of BNQDs was about 15 000 au (Figure 3C,a), and the i_{tot} obtained by the constant resistor-integrated BPE system (Figure 3B,a) was close to the i_{tot} without the resistor on the BPE (Figure S1A,a). When Fc-ssDNA was hybridized with H3 modified on the cathodic surface of BPE, the i_{tot} increased significantly (Figure 3B,b). On the one hand, due to the effects of the electron transfer and energy transfer of Fc and BNQDs, the ECL intensity of BNQDs was reduced to ~2000 au (Figure 3C,b). On the other hand, the ECL peak intensity of $[Ru(bpy)_3](PF_6)_2$ increased from 5400 (Figure 3D,a) to 15 700 au (Figure 3D,b). This signal enlargement could be attributed to the quantitative relationship in the circuit, which meant that the introduction of Fc facilitated the electron transfer rate of BPE, thus promoting the anode $[Ru(bpy)_3](PF_6)_2$ and TPrA reactions. In addition, the quenching effect of Fc for BNQDs and the enhancement effect for $[Ru(bpy)_3](PF_6)_2$ were compared with the BPE without a constant resistor system. The ECL intensity of BNQDs decreased by 92.18 and 89.49% (Figure S1B), respectively, while the ECL intensity of $[Ru(bpy)_3](PF_6)_2$ increased by 1.92 and 1.56 times (Figure S1C), respectively. This meant that the constant resistor was connected in parallel with the cathodic reservoir, resulting in lower total resistance and stronger i_{tot} (Figure 3B,c), thus triggering a stronger reaction behavior between $[Ru(bpy)_3](PF_6)_2$ and TPrA compared to the BPE without the resistor system (Figure S1A,c). Finally, after the dsDNA initiated by 10^{-14} M miRNA-141 was incubated on the cathode of BPE, the yellow-green emission of BNQDs was partially recovered. At the same time, the anodic emission of $[Ru(bpy)_3](PF_6)_2$ decreased, which was attributed to the decreasing electron transfer on BPE. Compared to BPE without a constant resistor system, the sensing platform exhibited higher sensitivity at the anode of BPE.

Detection of Target miRNA-141. The ECL signals of BNQDs and $[Ru(bpy)_3](PF_6)_2$ were related to the concen-

https://doi.org/10.1021/acs.analchem.1c04971
Anal. Chem. 2022, 94, 4303−4310

tration of miRNA-141. Therefore, it was possible to detect miRNA-141 through the changes of visual ECL intensity quantitatively. The ECL assay of the biosensor was carried out under the optimized conditions, and the visual image is shown in Figure 4. Since only $[Ru(bpy)_3](PF_6)_2$ emitted light when the miRNA-141 concentration was lower than 10^{-14} M, the variation of red bands was used to quantify. It was clear that the ECL of $[Ru(bpy)_3](PF_6)_2$ gradually weakened as the concentration of the target increased from 0 to 5×10^{-15} M. Figure 5A shows the ECL intensity−concentration curve. The linear equation (Figure 5B) was $y = -45.27 \lg C - 415.17$, with $R^2 = 0.991$. Figure 5C indicates the relationship between different concentrations of miRNA-141 and ECL intensities from BNQDs and $[Ru(bpy)_3](PF_6)_2$. The ECL emission of BNQDs became brighter and $[Ru(bpy)_3](PF_6)_2$ turned darker as the concentration of miRNA-141 increased from 10^{-14} to 10^{-7} M. To improve the accuracy of detection, the ratio method was adopted for quantitative analysis. As revealed in Figure 5D, the ratio of BNQDs to $[Ru(bpy)_3](PF_6)_2$ was proportional to the concentrations of miRNA-141. The linear fitting equation was $y = 1.938 + 0.092 \lg C$, with $R^2 = 0.991$. The dynamic range of our constructed sensor was 10 aM to 100 nM. According to previous reports, the cutoff concentration of miRNA-141 in prostate disease is 10^{-14} M.[24] Only one signal could be observed when the concentration was below the cutoff value, indicating that the patient was normal and the concentration of miRNA-141 could be calculated by linear equation (eq 1) ($y = -45.27 \lg C - 415.17$). The sensor displayed two signals when the target concentration was equal to and greater than the cutoff value, warning that the patient has prostate disease, and the concentration of miRNA-141 could be calculated by linear equation (eq 2) ($y = 1.938 + 0.092 \lg C$). Thus, the sensor we constructed would provide an accurate and intuitive result within the relevant physiological range. It was worth noting that, compared with the previous works, our prepared biosensor exhibited an excessive potential for ultrasensitive detection of miRNA-141 because of its low detection limit (10 aM) and wide linear range (10 aM to 100 nM, Table S3).

CONCLUSIONS

In summary, a visual ECL ratiometric biosensor based on a constant resistor-integrated BPE was constructed to realize the intuitive, accurate, and ultrasensitive detection of miRNA-141. This strategy only needed to insert a constant resistor into the BPE system without cumbersome sample preparation steps, making the total resistance of the whole circuit smaller. Under the driving voltage, a detection sensitivity of 10^{-17} M and a linear range of 10^{-17}−10^{-7} M could be achieved, which significantly improved the detection quality. In addition, the technology could be used to distinguish prostate disease: when the detection result had only one red band, it meant that the sample was normal human serum. As a result, it had both red and yellow-green bands simultaneously, and it warned that humans might have prostate disease, providing great application potential for the diagnosis and early treatment of prostate cancer.

ASSOCIATED CONTENT

Supporting Information

The Supporting Information is available free of charge at https://pubs.acs.org/doi/10.1021/acs.analchem.1c04971.

Reagents; instruments; cell culture and lysis; CV and ECL intensity for BPE without a resistor; selectivity and reproducibility of ECL biosensors; mechanistic study of $[Ru(bpy)_3](PF_6)_2$/TPrA; mechanism of BNQDs/$S_2O_8^{2-}$; optimal conditions of the ECL biosensor; comparison of driving potential; comparison of different methods for miRNA-141 detection; and application of the proposed biosensor (PDF)

AUTHOR INFORMATION

Corresponding Authors

Chuan-Xiang Chen − *College of Environmental and Chemical Engineering, Jiangsu University of Science and Technology, Zhenjiang 212100, P. R. China*; Phone: +86-511-84401181; Email: cxchen@just.edu.cn; Fax: +86-511-85635850

Yong-Hong Hu − *College of Food Science and Light Industry, Nanjing Tech University, Nanjing 211800, P. R. China*; orcid.org/0000-0002-8268-8763; Email: yonghonghuyg@163.com

Yin-Zhu Wang − *College of Environmental and Chemical Engineering, Jiangsu University of Science and Technology, Zhenjiang 212100, P. R. China; College of Food Science and Light Industry, Nanjing Tech University, Nanjing 211800, P. R. China*; orcid.org/0000-0002-7162-5556; Email: wangyz@just.edu.cn

Authors

Jie Zhao − *College of Environmental and Chemical Engineering, Jiangsu University of Science and Technology, Zhenjiang 212100, P. R. China; College of Food Science and Light Industry, Nanjing Tech University, Nanjing 211800, P. R. China*

Jia-Wan Zhu − *College of Environmental and Chemical Engineering, Jiangsu University of Science and Technology, Zhenjiang 212100, P. R. China*

Hui-Long Zong − *College of Environmental and Chemical Engineering, Jiangsu University of Science and Technology, Zhenjiang 212100, P. R. China*

Complete contact information is available at: https://pubs.acs.org/10.1021/acs.analchem.1c04971

Notes

The authors declare no competing financial interest.

ACKNOWLEDGMENTS

The authors are grateful for the financial support from the National Natural Science Foundation of China (Grant No. 21904050) and the Natural Science Foundation of Jiangsu Province, China (Grant No. BK20190952). This work also was supported by the Open Foundation of State Key Laboratory of Life Analytical Chemistry, Nanjing University (SKLACLS1912).

REFERENCES

(1) Sun, Y.; Fang, L.; Zhang, Z.; Yi, Y.; Liu, S.; Chen, Q.; Zhang, J.; Zhang, C.; He, L.; Zhang, K. *Anal. Chem.* **2021**, *93*, 7516−7522.

(2) Hu, J.; Li, Z.; Zhang, H.; Liu, R.; Lv, Y. *Anal. Chem.* **2020**, *92*, 8523−8529.

(3) Wang, F.; Liu, Y.; Fu, C.; Li, N.; Du, M.; Zhang, L.; Ge, S.; Yu, J. *Anal. Chem.* **2021**, *93*, 1702−1708.

(4) Chen, X.; Xu, K.; Li, J.; Yang, M.; Li, X.; Chen, Q.; Lu, C.; Yang, H. *Biosens. Bioelectron.* **2020**, *155*, No. 112104.

(5) Meng, S.; Chen, R.; Xie, J.; Li, J.; Cheng, J.; Xu, Y.; Cao, H.; Wu, X.; Zhang, Q.; Wang, H. *Biosens. Bioelectron.* **2021**, *190*, No. 113470.
(6) Oliveira, G. P., Jr.; Barbosa, R. H.; Thompson, L.; Pinckney, B.; Murphy Thornley, M.; Lu, S.; Jones, J.; Hansen, C. H.; Tigges, J.; Wong, W. P.; Ghiran, I. C. *Biosens. Bioelectron.* **2021**, *189*, No. 113307.
(7) Wang, J.; Cai, K.; Zhang, R.; He, X.; Shen, X.; Liu, J.; Xu, J.; Qiu, F.; Lei, W.; Wang, J.; Li, X.; Gao, Y.; Jiang, Y.; Xu, W.; Ma, X. *Anal. Chem.* **2020**, *92*, 9399−9404.
(8) Lu, L.; Zhang, L.; Miao, W.; Wang, X.; Guo, G. *Anal. Chem.* **2020**, *92*, 9613−9619.
(9) Cai, W. R.; Zhang, G. Y.; Lu, K. K.; Zeng, H. B.; Cosnier, S.; Zhang, X. J.; et al. *ACS Appl. Mater. Interfaces* **2017**, *9*, 20904−20912.
(10) Dong, J.; Lu, Y.; Xu, Y.; Chen, F.; Yang, J.; Chen, Y.; Feng, J. *Nature* **2021**, *596*, 244−249.
(11) Ma, Y.; Colin, C.; Descamps, J.; Arbault, S.; Sojic, N. *Angew. Chem., Int. Ed.* **2021**, *60*, 18742−18749.
(12) Liang, Z.; Zhang, Q.; Nie, Y.; Zhang, X.; Ma, Q. *Anal. Chem.* **2020**, *92*, 9223−9229.
(13) Fu, X.; Tan, X.; Yuan, R.; Chen, S. *Biosens. Bioelectron.* **2017**, *90*, 61−68.
(14) Zhang, Y.; Xu, J.; Zhou, S.; Zhu, L.; Lv, X.; Zhang, J.; Zhang, L.; Zhu, P.; Yu, J. *Anal. Chem.* **2020**, *92*, 3874−3881.
(15) Zhang, H. R.; Wang, Y. Z.; Zhao, W.; Xu, J. J.; Chen, H. Y. *Anal. Chem.* **2016**, *88*, 2884−2890.
(16) Ismail, A.; Voci, S.; Pham, P.; Leroy, L.; Maziz, A.; Descamps, L.; Kuhn, A.; Mailley, P.; Livache, T.; Buhot, A.; Leichle, T.; Bouchet-Spinelli, A.; Sojic, N. *Anal. Chem.* **2019**, *91*, 8900−8907.
(17) Bouffier, L.; Manojlovic, D.; Kuhn, A.; Sojic, N. *Curr. Opin. Electrochem.* **2019**, *16*, 28−34.
(18) Peng, D.; Zhang, L.; Li, F. F.; Cui, W. R.; Liang, R. P.; Qiu, J. D. *ACS Appl. Mater. Interfaces* **2018**, *10*, 7315−7323.
(19) Yang, X. Y.; Wang, Y. Z.; Wang, L. L.; Zhu, J. W.; Zhao, J.; Zong, H. L.; Chen, C. X. *Biosens. Bioelectron.* **2021**, *191*, No. 113393.
(20) Peng, C.; Xing, H.; Fan, X.; Xue, Y.; Li, J.; Wang, E. *Anal. Chem.* **2019**, *91*, 5762−5767.
(21) Lu, H. J.; Zhao, W.; Xu, J. J.; Chen, H. Y. *Biosens. Bioelectron.* **2018**, *102*, 624−630.
(22) Peng, H.; Huang, Z.; Deng, H.; Wu, W.; Huang, K.; Li, Z.; Chen, W.; Liu, J. *Angew. Chem., Int. Ed.* **2020**, *59*, 9982−9985.
(23) Wang, N.; Wang, Z.; Chen, L.; Chen, W.; Quan, Y.; Cheng, Y.; Ju, H. *Chem. Sci.* **2019**, *10*, 6815−6820.
(24) Wang, Y. Z.; Ji, S. Y.; Xu, H. Y.; Zhao, W.; Xu, J. J.; Chen, H. Y. *Anal. Chem.* **2018**, *90*, 3570−3575.
(25) Zhang, R.; Cheng, J.; Yang, L.; Wong, J. M.; Ralph Adsetts, J.; Wang, R.; Liu, J.; Ding, Z.; Wang, H. B. *ChemElectroChem* **2021**, *8*, 547−557.
(26) Lee, J. I.; Choi, H.; Kong, S. H.; Park, S.; Park, D.; Kim, J. S.; Kwon, S. H.; Kim, J.; Choi, S. H.; Lee, S. G.; Kim, D. H.; Kang, M. S. *Adv. Mater.* **2021**, *33*, No. 2100321.
(27) Zhang, X.; Zhou, Y.; Chai, Y.; Yuan, R. *Anal. Chem.* **2021**, *93*, 7987−7992.
(28) Hao, Q.; Xu, Q.; Niu, S.; Ding, C.; Luo, X. *Anal. Chem.* **2021**, *93*, 10679−10687.
(29) Deng, H.; Chai, Y.; Yuan, R.; Yuan, Y. *Anal. Chem.* **2020**, *92*, 8364−8370.
(30) Deng, K.; Xiao, J.; Liu, Z.; Li, C.; Wang, J.; Yi, Q.; Huang, H.; Zhou, H. *Biosens. Bioelectron.* **2021**, *181*, No. 113152.
(31) Xia, L. Y.; Li, M. J.; Wang, H. J.; Yuan, R.; Chai, Y. Q. *Anal. Chem.* **2020**, *92*, 14550−14557.
(32) Jiang, X.; Wang, H.; Wang, H.; Zhuo, Y.; Yuan, R.; Chai, Y. *Anal. Chem.* **2017**, *89*, 4280−4286.
(33) Wang, Y. Z.; Xu, C. H.; Zhao, W.; Guan, Q. Y.; Chen, H. Y.; Xu, J. J. *Anal. Chem.* **2017**, *89*, 8050−8056.
(34) Liu, B.; Yan, S.; Song, Z.; Liu, M.; Ji, X.; Yang, W.; Liu, J. *Chem. − Eur. J.* **2016**, *22*, 18899−18907.
(35) Qin, D.; Jiang, X.; Mo, G.; Feng, J.; Deng, B. *Electrochim. Acta* **2020**, *335*, No. 135621.
(36) Soulsby, L. C.; Doeven, E. H.; Pham, T. T.; Eyckens, D. J.; Henderson, L. C.; Long, B. M.; Guijt, R. M.; Francis, P. S. *Chem. Commun.* **2019**, *55*, 11474−11477.
(37) Liu, Y.; Wang, M.; Nie, Y.; Zhang, Q.; Ma, Q. *Anal. Chem.* **2019**, *91*, 6250−6258.
(38) Liu, Y.; Chen, X.; Wang, M.; Ma, Q. *Green Chem.* **2018**, *20*, 5520−5527.
(39) Shen, T.; Liu, S.; Yan, W.; Wang, J. *J. Mater. Sci.* **2019**, *54*, 8852−8859.
(40) Liang, Z.; Nie, Y.; Zhang, X.; Wang, P.; Ma, Q. *Anal. Chem.* **2021**, *93*, 7491−7498.
(41) Wu, A. H.; Sun, J. J.; Zheng, R. J.; Yang, H. H.; Chen, G. N. *Talanta* **2010**, *81*, 934−940.
(42) Shi, H. W.; Wu, M. S.; Du, Y.; Xu, J. J.; Chen, H. Y. *Biosens. Bioelectron.* **2014**, *55*, 459−463.

Recommended by ACS

Versatile Electrochemiluminescence Biosensing Platform Based on DNA Nanostructures and Catalytic Hairpin Assembly Signal Amplification

Linying Yu, Xiurong Yang, *et al.*
AUGUST 04, 2022
ANALYTICAL CHEMISTRY
READ

Boron Carbon Nitride Nanosheets-Ru Nanocomposite Self-Enhancement Electrochemiluminescence Emitter with a Three-Dimensional DNA Network Structure as a Signal...

Jicui Hu, Ruo Yuan, *et al.*
AUGUST 02, 2022
ANALYTICAL CHEMISTRY
READ

Plasmon-Enhanced Nitrogen Vacancy-Rich Carbon Nitride Electrochemiluminescence Aptasensor for Highly Sensitive Detection of miRNA

Shimeles Addisu Kitte, Yongdong Jin, *et al.*
DECEMBER 20, 2021
ANALYTICAL CHEMISTRY
READ

Sensitive Electrochemiluminescence Biosensor Based on the Target Trigger Difference of the Electrostatic Interaction between an ECL Reporter and the Electrode Surface

Yilei Lu, Zhenyu Lin, *et al.*
APRIL 06, 2022
ANALYTICAL CHEMISTRY
READ

Get More Suggestions >

https://doi.org/10.1021/acs.analchem.1c04971
Anal. Chem. 2022, 94, 4303−4310